Dalton Transactions

Accepted Manuscript

This is an *Accepted Manuscript*, which has been through the Royal Society of Chemistry peer review process and has been accepted for publication.

Accepted Manuscripts are published online shortly after acceptance, before technical editing, formatting and proof reading. Using this free service, authors can make their results available to the community, in citable form, before we publish the edited article. We will replace this *Accepted Manuscript* with the edited and formatted *Advance Article* as soon as it is available.

You can find more information about *Accepted Manuscripts* in the Information for Authors.

Please note that technical editing may introduce minor changes to the text and/or graphics, which may alter content. The journal's standard Terms & Conditions and the Ethical guidelines still apply. In no event shall the Royal Society of Chemistry be held responsible for any errors or omissions in this *Accepted Manuscript* or any consequences arising from the use of any information it contains.

ROYAL SOCIETY OF CHEMISTRY

www.rsc.org/dalton

Cite this: DOI: 10.1039/c0xx00000x

www.rsc.org/xxxxxx

ARTICLE TYPE

Enhanced Field Emission and Photocatalytic Performance of MoS_2 Titania Nanoheterojunctions via Two Synthetic Directions

Hao Fu, Ke Yu*, Honglin Li, Jinzhu Li, Bangjun Guo, Yinghua Tan, Changqing Song and Ziqiang Zhu

Received (in XXX, XXX) Xth XXXXXXXXX 20XX, Accepted Xth XXXXXXXXX 20XX

DOI: 10.1039/b000000x

Two kinds of MoS_2 titania nanoheterojunctions with different morphologies was synthesized via two different approaches. They are facile and additives free hydrothermal processes which would result high material productivity and controllable morphologies. The synthesis directions and their growth mechanisms were both discussed, meanwhile the field emission properties of MoS_2 titania nanoheterojunctions were investigated. The experimental data indicated that the MoS_2@TiO_2 heterojunctions had an excellent field emission performance with turn-on field of 2.2 $V\mu m^{-1}$ and threshold field of 3.6 $V\mu m^{-1}$ on Si substrate on account of the large quantities of sharp edges. Moreover, since a p-n heterojunctions was formed, the photocatalytic activities of both composites were evaluated by monitoring the photodegradation of methylene blue (MB). The result showed that the TiO_2@MoS_2 heterojunctions had better photocatalytic properties of 90% degradation within 100 minutes. The morphologies differences generated from different synthetic directions made a huge impact on the composites' properties.

1. Introduction

Titanium dioxide (TiO_2) has been widely investigated over the decades due to its excellent electronic and catalytic properties, which are high physical and chemical stability, strong oxidizing power, effectivity and non-toxicity.[1] Therefore, various applications of TiO_2 have been explored. But more importantly, it leads to the research efforts toward morphology control, crystal engineering and modification of TiO_2 which will guarantee a better application performance.[2-4] Among these morphologies, three dimensional TiO_2 nanostructure processes a great advantage in crystalline phase, specific surface area, sharp edges, scale-up production and synthetic route.[5] Nevertheless, the three dimensional TiO_2 nanostructure still has its limitations which are high electron–hole pairs' recombination, and inactive under visible light due to its wide band gap.[6] In order to avoid or resolve the aforementioned disadvantages, a variety of synthetic strategies has been considered, one of them is semiconductor heterojunctions.[7-10] By coupling different semiconductor with TiO_2, an enhanced performance can be achieved due to the decrease in electron-hole pairs' recombination as well as the increase in light region absorption region and active sharp edges. Molybdenum disulfide (MoS_2) has been a study focus for a long time regarding its graphene resembling properties, narrow band gap, excellent morphologies and its relevant applications like lithium battery, hydrogen storage, photocatalysis, sensors and field emission.[11-13] So far, a lot of MoS_2 morphologies and heterojunctions with great photocatalytic or field emission properties were successfully synthesized for the fact that increasing active sites and decreasing electron-hole pairs' recombination can be achieved by morphology control.[14-17] It is known that semiconductor heterojunctions is one of the most effective method to accomplish such improvement. And it is our contention that MoS_2 titania nanoheterojunctions is one of the best candidates for high application performance giving its great crystal modification potential in conductance, aspect radio, and ultrathin edges, which will eventually contribute to an excellent field emitter or photocatalytic material.

There are a few existing studies of MoS_2 titania heterojunctions with remarkable hydrogen evolution or lithium storage performance, but both required complex and difficult synthetic route.[18-20] It is our belief that not only the excellent morphology and application performance but also high yields fabrication with low difficulty should be considered as the main factors in nanoscale synthesis for further application. Giving that idea, we devoted a serious amount of time, trying to develop a simplified fabrication route without compromising the material's performance. In this work, two kinds of MoS_2 titania nanoheterojunctions with different morphologies was synthesized via two different facile hydrothermal processes. One of them is three dimensional TiO_2 based composite with waves-like MoS_2, which is defined as TiO_2@MoS_2, and the other is MoS_2 nanoflowers based composite with TiO_2 nanoparticles which is defined as MoS_2@TiO_2. Unlike the TiO_2@MoS_2 composites in other works we just mentioned, in our experiment, we manage to

Dalton Transactions Accepted Manuscript

let the MoS_2 nanosheets to grow separately rather than enwrapping on the TiO_2 nanorods in order not only to increase the exposed active surface of both TiO_2 and MoS_2 but also achieve excellent heterojunction characteristic. We successfully developed better performances as well as larger surface areas in this two heterojunctions comparing our pre-existing finding.[21] Excellent field emission properties of MoS_2@TiO_2 nanoheterojunctions were also obtained for the first time due to the increased sharp edges which would verify our hypothesis in the first place. Since the light absorption region had also been increased, and a p-n junction had been formed, we evaluated their photocatalytic activities by monitoring the photodegradation of methylene blue (MB), which also had been enhanced. Both morphology differences resulting from diverse synthetic direction and their impact on application performance will be discussed.

2. Experimental section

2.1 Synthesis of MoS_2@TiO_2 heterojunctions

The chemical reagents used in this work were analytical grade without further purification. 1 g $Na_2MoO_4 \cdot 2H_2O$, 1.4 g thioacetamide and 0.33 g oxalic acid were dissolved in a breaker with 80 mL deionized water, stirred for 10 minutes, then transferred into a 100 mL stainless-steel Teflon lined autoclave, and heated at 200 centigrade for 24 hours. The pure black MoS_2 precipitate were filtered, washed with deionized water and dried at 60 centigrade for 6 hours. 1 mL of 35% HCl and 2 mL of TBOT (titania butoxide) was doped on 0.5 g aforementioned obtained MoS_2 successively. After it cooled down, the mixture was dispersed in 20 mL of oleic acid, stirred for 10 minutes, transferred to a 50 mL stainless-steel Teflon lined autoclave, and then heated at 180 centigrade for 4 hours. The MoS_2@TiO_2 heterojunctions was eventually collected, washed with absolute ethanol, dried at 60 centigrade for 1 hour and annealed at 850 centigrade for 2 hours in argon for further characterization.

2.2 Synthesis of TiO_2@MoS_2 heterojunctions

4 mL of TBOT (titania butoxide) was mixed with 2 mL of 35% HCl in a conical flask, after it cooled down, the mixture was doped slowly into 20mL of oleic acid, then stirred for 10 minutes. Afterward, the resultant was transferred in to a 50 mL stainless-steel autoclave with a Teflon liner and heated at 180 centigrade for 4 hours. Then the pure TiO_2 product was collected from the bottom, washed with absolute ethanol, and dried at 60 centigrade for 1 hour. 0.5 g $Na_2MoO_4 \cdot 2H_2O$, 0.7 g thioacetamide, 0.4 g oxalic acid, and 1.5g the aforementioned obtained TiO_2 were dissolved in a breaker with 70 mL deionized water. The solution was stirred for 10 minutes then transferred to a 100 mL stainless-steel Teflon lined autoclave heated at 200 centigrade for 24 hours. At last, the precipitate was collected and washed with deionized water, and dried at 60 centigrade for 6 hours to obtain TiO_2@MoS_2 heterojunctions, the sample was annealed at 850 centigrade for 2 hours in argon for further characterization.

2.3 Characterization

The crystal structure of the samples was characterized by X-ray diffraction (XRD, Bruker D8 Advance diffractometer) by using monochromatized Cu-K radiation. The diffraction patterns were gathered in the 2 scanning range from 10 to 80 with 0.02 per step. The structure and morphologies were characterized via field emission scanning electron microscopy (FESEM, JEOL-JSM-6700F) at an accelerating voltage of 20 kV and transmission electron microscopy (TEM, JEOL-JEM-2110) at an accelerating voltage of 200 kV. Before TEM characterization, a minimum amount of sample was dispersed in 8 mL of ethanol and under ultrasonication for 20 minutes. A dope of the colloidal solution was added onto a copper micro grid which afterward was dried in air at room temperature for TEM characterization.

2.4 Field emission measurement

In the field emission experiment, the as-prepared samples were screen-printed on the silicon substrate, and dried in vacuum at 50 centigrade for 5 hours to serve as cathode with a measured emission area of 1×1 cm^2, which was also separated from a phosphor-indium tin oxide (ITO)/glass anode by two Teflon spacers with a thickness of 200 μm. A vacuum chamber with a high vacuum level of 5×10^{-5} Pa was established to perform field emission measurement at room temperature. During the experiment, the turn-on field and the threshold field are defined as the field produces a current density of 1 μAcm^{-2} and 0.1$mAcm^{-2}$ respectively.

2.5 Photocatalytic measurements

The methylene blue was chosen in this experiment duo to its strong adsorption to metal oxide surface as well as great stability under different pH conditions. The characteristic peak of 666 nm was used to monitor the concentration of the solution in this experiment at room temperature. 0.01 g of the each sample was added to a cylindrical container with 100 mL MB aqueous solution (10 mg L^{-1}). The solution was kept in dark and stirred for 20 min to establish the adsorption-desorption equilibrium before irradiation. In order to reduce the heat effect, the reactor was placed in a glass container which was cooling by flowing water. A 20 W tungsten halogen lamp was served to provide irradiation, the absorption spectra of MB was analyzed via UV-vis spectrophotometer (UNICO 2802) every 20 minutes.

3. Result and discussion

3.1 characterization and morphology

The XRD patterns of the as-prepared samples are showed in Fig. 1 (a), pure MoS_2 and TiO_2 were assigned to the pure hexagonal phase of MoS_2 (JCPDS 37-1492) and rutile phase of TiO_2 (JCPDS 21-1276) respectively. On regarding of the two kind of MoS_2 titania heterojunctions, each main characteristic peak of pure TiO_2 can be observed in both kinds, but in contract, the main characteristic peaks of MoS_2 can be only observed clearly in the MoS_2@TiO_2 composites, which can be explained by the crystallinity difference between MoS_2 and titania, as well as the less amounts of MoS_2 in the TiO_2@MoS_2 composites. It is worth mentioning that the (001) plane of TiO_2 in the TiO_2@MoS_2 composites is much stronger than MoS_2@TiO_2 composites, indicating the large percentage of active TiO_2 (001) plane in crystal structure. As shown in Fig. 1 (b), we construct the diagram of MoS_2, TiO_2 and heterojunction structure. The

Dalton Transactions Accepted Manuscript

This journal is © The Royal Society of Chemistry [year]

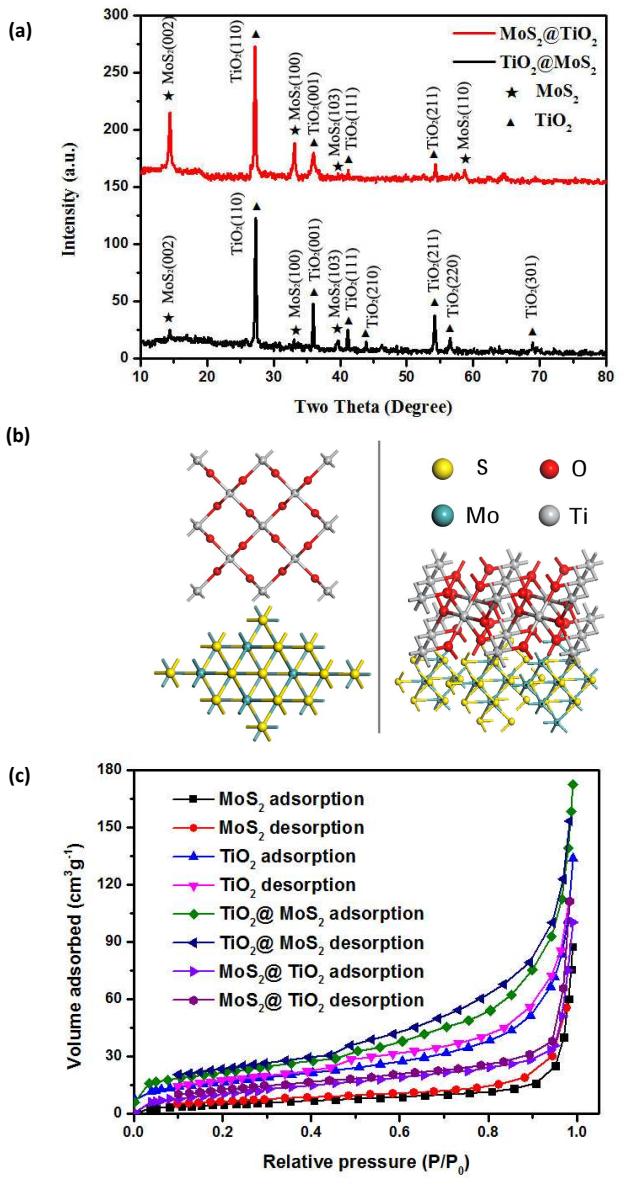

Fig. 1 (a) The X-ray diffraction patterns of TiO_2@MoS_2 heterojunctions (red curve), MoS_2@TiO_2 heterojunctions (black curve). Each visible diffraction peak was marked with corresponding symbol. (b) The atomic structure of MoS_2 and TiO_2. (c) Nitrogen adsorption-desorption isotherms of four samples.

synthesized MoS_2 belongs to Hexagonal with P63/mmc(194) space groups and TiO_2 belongs to Tetragonal with P42/mnm(136) space group. Fig. 1 (c) is the nitrogen adsorption-desorption isotherm of four samples, we identified two distinct hysteresis loops at a relative pressure of 0.1-0.9. The Brunauer-Emmett-Teller (BET) surface area for MoS_2, TiO_2, MoS_2@TiO_2 and TiO_2@MoS_2 are 20.3 $m^2 g^{-1}$, 71.4 $m^2 g^{-1}$, 25.1 $m^2 g^{-1}$, and 79.8 $m^2 g^{-1}$, respectively. The MoS_2@TiO_2 and TiO_2@MoS_2 heterojunction structures showed an obvious improvement comparing to the pure MoS_2 and TiO_2.

In order to study the morphologies as well as the growth mechanisms of all the samples, FESEM and TEM were also performed. As we can see in Fig. 2 (a), the morphology of MoS_2

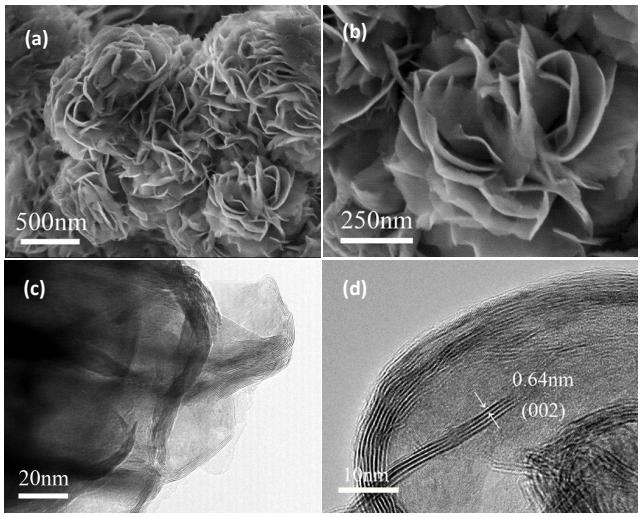

Fig. 2 (a) (b) SEM images of MoS_2 nanoflowers with medium and high magnification. (c) TEM image of MoS_2 petals under medium magnification. (d) TEM image of a MoS_2 petal individual under high magnification.

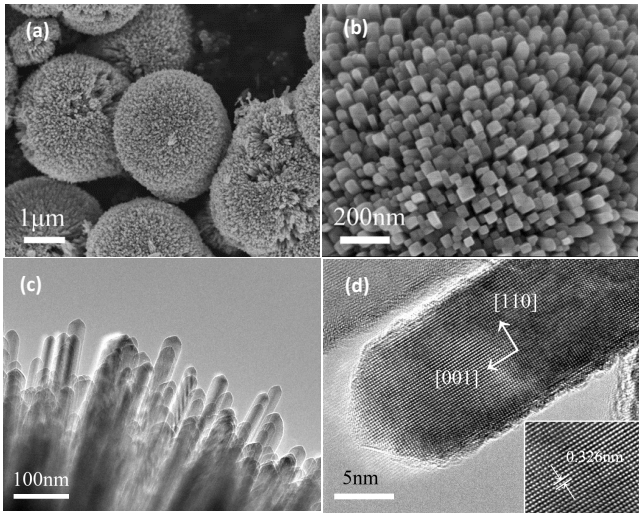

Fig. 3 (a) (b) SEM images of TiO_2 with medium and high magnification. (c) TEM image of TiO_2 nanorods under medium magnification. (d) TEM image of a TiO_2 rod individual under high magnification. The inset is a HRTEM image with a clear observation of lattice distance.

can be described as a flower-like sphere which is assembled by a large amount of petals therefore was called nanoflower. Fig. 2 (b) is a high magnification SEM image, which showed that every petal is aligned together with a common inter center, formed a spherical MoS2 with an average diameter of 1 to 2 μm. Fig. 2 (c) and (d) are the TEM images with medium and high magnification, each so called petal is clearly constructed by 5-9 MoS_2 single layer nanosheets with an interlayer separation of 0.64 nm, which can be assigned to the (002) plane. On the other hand, Fig. 3 (a) is the SEM image of TiO_2 with medium magnification which indicates the spherical structure of TiO_2 with an average diameter of 2 μm, Fig. 3 (b) showed the radiant aggregation of nanorods, which is further clearly observed in Fig. 3 (c). Fig. 3 (d) demonstrated the TEM image of a single nanorod individual, which have a unique shape of triangle end with an average diameter of 15 nm, and length of 1 μm. The distance between the

Dalton Transactions Accepted Manuscript

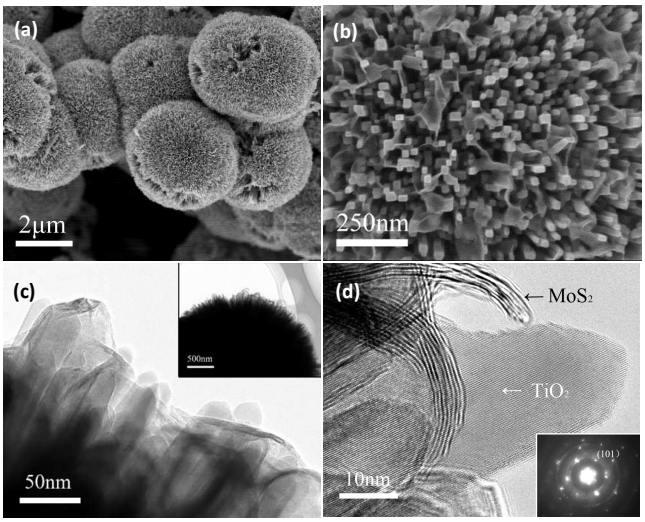

Fig. 4 (a) (b) SEM images of TiO_2@MoS_2 composites with low and medium magnification. (c) TEM image of TiO_2@MoS_2 composites edges under medium magnifications. The inset is the TEM image of TiO_2@MoS_2 composites under low magnification. (d) High magnification TEM image with a clear observation of MoS_2 and TiO_2 combination. The insert shows the SAED image of the TiO_2 rod.

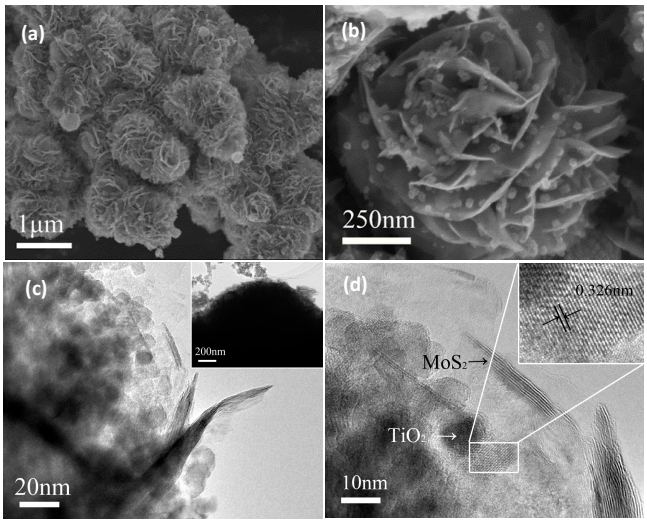

Fig. 5 (a) (b) SEM images of MoS2@TiO_2 composites with low and medium magnifications. (c) TEM image of MoS_2@TiO_2 composites edges under medium magnification. The Inset is the TEM image of MoS_2@TiO_2 composites under low magnification. (d) High magnification TEM image with a clear observation of MoS_2 and TiO_2 combination. The inset shows an HRTEM image corresponding to the selected area within a white rectangle.

adjacent lattice fringes was measured to be 0.326 nm, which is consistent with the interplanar distance of rutile TiO_2 (001), indicating the growth direction of [001], parallel to c-axis.

Comparing to the petal-like multiple layers of MoS_2 nanoflower, in the TiO2@MoS2 composites, the MoS2 grown perpendicularly and uniformly on the TiO_2 surface. Fig. 4 (a) showed the MoS_2 layers aggregated to the center of the TiO_2 sphere, forming a waves-like morphology. Fig. 4 (b) is SEM image with medium magnification, showed that the MoS_2 waves run through the gaps between TiO_2 nanorods. We can clearly see the structure mixture of the nanorods and nanosheets of TiO_2 and MoS_2 respectively from Fig. 4 (c). Each wave on the TiO_2 surface is a single nanosheet which is consist of 5-9 MoS_2 layers just like the petal in pure MoS_2 nanoflowers, which can be concluded from Fig. 4 (d). The inset of Fig. 4 (d) gives the selected-area electron diffraction (SAED) pattern of a single TiO_2 nanorod in the TiO_2@MoS_2 composites, which can confirm the single-crystalline structure of TiO_2 rutile. In the MoS_2@TiO_2 composites, the TiO_2 nanoparticles were homogeneous dispersed both outside and inside the MoS_2 nanoflowers, MoS_2-based structure can be seen in Fig. 4 (a) and (b), the TEM images of MoS_2@TiO_2 composites which are Fig. 4 (c) and (d), showed the fact that each TiO_2 nanoparticle with a diameter of 10 nm is adhered on the MoS_2 petal. The lattice distance of a TiO_2 nanoparticle was clearly measured to be 0.326 nm via HRTEM image (inset in Fig. 5 (d)), also corresponding to the (001) plane of TiO_2 rutile. From the TEM images of both composites, not only the MoS_2 multiple layers and TiO_2 nanorods/nanoparticles can be observed, but also the adjacent lattice fringes of TiO_2 and separation distance of MoS_2 layers are consistent with the aforementioned finding in pure TiO_2 nanorods and MoS_2 as well.

The growth mechanism of MoS_2 nanoflowers can be easily described as the aggregation of multiple layers petals, the $Na_2MoO_4{\cdot}2H_2O$ and thioacetamide served as Mo and S sources respectively, and the oxide acid was used to adjust the pH value below 1 to accelerate the hydrolysis of thiourea as well as to decrease the solubility of MoS_2 nanosheets.[22-24] The laminar growth habit of MoS_2 contributed the center aggregation, and finally grow into flower nanostructure. In terms of the pure TiO_2 nanosphere, the growing process can be actually divided into three stages.[25] First of all, the water and non-polar solvent form an interface between two immiscible fluids which is an ideal environment for 3D nanostructure for the fact that nanoparticles can be highly mobile and achieve equilibrium assembly at the interface. In our case, the HCl and oleic acid provided the water and solvent respectively, and TBOT hydrolyze to form titania nucleus as titanium precursor. In the second stage, the nucleus evolved along the [001] orientation on the account of acid environment and selective adsorption of Cl^- on the TiO_2 nucleus contribute to the anisotropic growth of nanorods. The adsorption of Cl^- on the (001) plane generate a repulsive force between the nanorods which incline to aggregate on the (001) plane, and consequently create the core of nanosphere. Finally, the nanorods further grown and radial assembled as a spherical structure to reduce their total free energy. It is worth mentioning that each individual TiO_2 nanorod has the large area of highly reactive (001) plane which is the most reactive facet in three fundamental low-index facets exposed in TiO_2 crystals.[26]

However, the TiO_2 nanoparticles which were dispersed on the MoS_2 petals in the MoS_2@TiO_2 composites are actually the initial stage of TiO_2 nanorods. By halving the amount of sufficient reagent to synthesize pure TiO_2 in the experiment section, the TiO_2 can remain the particle stage while we adjust the amounts of MoS_2 to create the best morphology. Fig. 6 (a) – (c) showed the TiO_2 nanoparticles tend to evolve from scattered to be clustered in the MoS_2@TiO_2 composites with the variable of MoS_2 amounts from 1g to 0.3g. When 0.5g of MoS_2 was added, the TiO_2 nanoparticles had the best homogeneous dispersion on the

Dalton Transactions Accepted Manuscript

This journal is © The Royal Society of Chemistry [year]

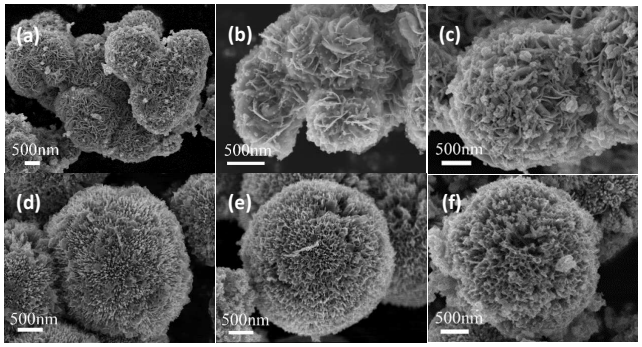

Fig. 6 (a) (b) (c) SEM images of MoS_2@TiO_2 composites synthesized with 1g, 0.5g and 0.3g amounts of MoS_2. (d) (e) (f) SEM images of TiO_2@MoS_2 composites synthesized with 0.4g, 0.7g and 1g amounts of thiourea.

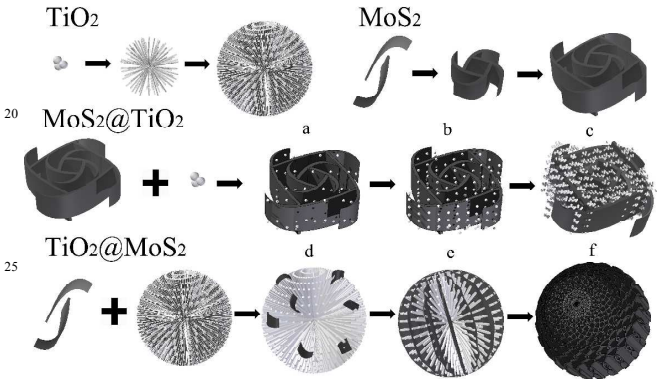

Scheme 1 Schematic illustration of growth mechanisms. The black and silver represent MoS_2 and TiO_2 respectively.

MoS_2 surface, thus it further proved that the synthesis of MoS_2@TiO_2 composites is a simple combination of two materials with a purpose of utilizing the nanoparticles which can be served as active sharp points for field emission applications. For another synthesis direction, the TiO_2@MoS_2 composites have the completed TiO_2 morphology. Unlike simple combination, MoS_2 grown wave-like on the TiO_2 surface, and developed the same aggregation center as TiO_2. Waves-like MoS_2 grown perpendicularly on nanorods-constructed TiO_2 nanosphere with high percentage of {001} facets rather than simple enwrapping MoS_2 layers on the TiO_2 surface also by decreasing the amount of sufficient reagent to synthesize pure MoS_2 in the experiment section. In this synthesis direction, thiourea served not only as the sulfur source for the MoS_2 formation, but also an effective coupling agent to link the MoS_2 nanosheets to the TiO_2 surface.[27] Therefore, serial experiments with different amount of thiourea were performed in order to study the growth mechanism of TiO_2@MoS_2 composites. When 0.4g of thiourea was added, a small amount of MoS_2 nanosheets was attached to the spherical surface. (Fig. 6 (d)) By increasing the amount of thiourea to 0.7g, the MoS_2 nanowaves were formed, run through the nanorods about same height, and the morphology became unified. (Fig. 6 (e))When thiourea was 1g, the MoS_2 nanowaves connected together, evolved radially, and finally overlapped the TiO_2 sphere, (Fig. 6 (f)) indicating the excessive growth of MoS_2. Based on the above descriptions, we constructed Scheme 1 which is a comprehensive growth evolution illustration of MoS_2, TiO_2, TiO_2@MoS_2 and MoS_2@TiO_2, the black and silver represent the MoS_2 and TiO_2, and the stage (a) – (f) in the scheme match with Fig. 6 (a) – (f) respectively. The three stages of pure TiO_2 nanosphere and the aggregation of MoS_2 multiple layers petals are clearly illustrated in the scheme, meanwhile the idea of reducing the dosage of reactants to limit the morphologies of MoS_2 and TiO_2 at their primary stages then use to construct composites via two different synthesis directions are also showed.

3.2 Field emission study

The measurement method of field emission property had been described in the experimental section. Fig. 7 (a) shows the field emission current density-applied field (J-E) curves for several bias voltage sweep of four samples. The turn-on and threshold field of the TiO_2-based TiO_2@MoS_2 composites has been decreased from 3.1 $V\mu m^{-1}$ and 7.2 $V\mu m^{-1}$ to 2.5 $V\mu m^{-1}$ and 4.5 $V\mu m^{-1}$ comparing to the pure TiO_2 nanorods, the MoS_2-based MoS_2@TiO_2 composites has been decreased from 4 $V\mu m^{-1}$ and 6.1 $V\mu m^{-1}$ to 2.2 $V\mu m^{-1}$ and 3.6 $V\mu m^{-1}$ comparing to the pure MoS_2 nanoflowers. A good repeatability can also be concluded from the several sweeps in J-E curves. The overall J-E curve exhibits a fact that the MoS_2@TiO_2 composites owned the best enhanced field emission property among all the samples, which further verified that the morphology of sample made a huge impact on the field emission performance for the fact that the vastly distributed nanoparticles which serve as sharp edge, can dramatically increase the emission points as well as field enhancement factor. The mechanism of this field emission enhancement in MoS_2@TiO_2 composites had been illustrated in Fig. 7 (d). The black curves above the MoS_2 petal represent the electrostatic field, the electric potential gradient has been improved after the adding of TiO_2 nanoparticles, furthermore, the local field strength predominates, the emission current on the top of nanoparticles become stronger than the single MoS_2 petal, making it easier to emit to the vacuum.[28] Based on this theory, the vast distribution of nanoparticles can be considered as an effective coupling method in field emission material synthesis.

The Fowler-Nordheim (F-N) plot corresponding to four samples has been shown in Fig. 7 (b). The dots basically line up straight indicating that the emitting electrons were mainly generated from barrier tunneling electrons which were excited by the electric field. The field emission characteristic was analyzed via the Fowler-Nordheim equation below:

$$\ln (J/E^2) = \ln (A\beta^2/\varphi) - (B\varphi^{3/2})/\beta E \qquad (1)$$

Where J and E stand for the emission current density and applied electric field respectively. A and B are constant with the value of 1.56×10^{-10} (AV^{-2} eV) and 6.830×10^{3} ($eV^{-3/2}V\mu m^{-1}$), while φ and β represent the work function and the field enhancement factor of the materials. According to the F-N plot as well as the equation, the enhancement factor can be hence calculated via:

$$\beta = -B\varphi^{3/2}/k_{slope} \qquad (2)$$

Based on the previous research, the work function of TiO_2 is 4.5 eV,[6] and we estimated the work function of MoS_2 is about 4.52 eV,[29] therefore the enhancement factor for MoS_2 and TiO_2 are obtained to be 1640 and 3725 respectively. The data shows the

Dalton Transactions Accepted Manuscript

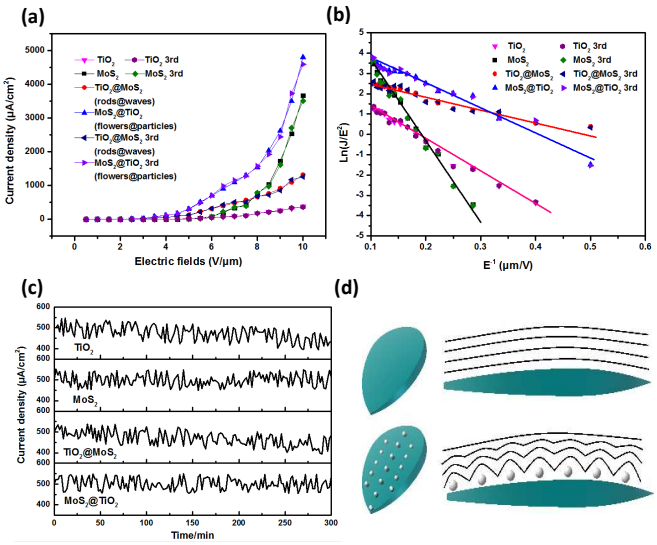

Fig. 7 The field emission property comparisons of MoS_2, TiO_2, TiO_2@MoS_2, and MoS_2@TiO_2 (a) The dependence of the current density J on the applied electric field E for several bias voltage sweeps. (b) The Fowler-Nordheim (F-N) plot. (c) The emission stability measurement with an emission density of 500 μA cm^{-1}. (d) The equipotential maps of electrostatic field in the cases of a pure MoS_2 petal and MoS_2@TiO_2

fact that TiO_2 do have the lower work function and higher enhancement factor, but with a lack of field emission performance, which can be attributed to the field shielding effect, so high that the electrostatic field became impossible to bend over. The high density of TiO_2 nanorods can also be verified in the SEM images of pure TiO_2 and TiO_2@MoS_2 as well.

Generally, the field enhancement factor β is largely depended on emitter geometry, crystal structure, work function, screen effect, vacuum gap, and the spatial distribution of emitting centres.[14] In the MoS_2@TiO_2 composites, the formation of p-n heterojunctions at the interface also contribute to this enhancement. Electrons transfer occurred to establish thermal equilibrium, align their Fermi levels, and due to carrier concentration gradients, electrons flow from TiO_2 to MoS_2 to form a negative charge, while holes flow from MoS_2 to TiO_2 to form a positive charge which eventually lead to an opposing electric field at the junction. When MoS_2@TiO_2 composites were used as cathode, this built-in electric field and applied field both had the same direction. The electrons in the MoS_2 nanoflowers therefore can easily transfer to the TiO_2 nanoparticles, and tunnel to emit at the vacuum level afterward. To sum up, the enhancement factor was improved on account of the multistage geometry as well as the formation of heterojunctions structure.

In addition, the field emission stability measurement of all the samples was also performed via plotting the emission current density versus time with a start value of 500 μAcm^{-1}. As we can see from Fig. 7 (c), a trend of decrease can be observed in pure TiO_2 and TiO_2@MoS_2 composites after 150 min, meanwhile, the current density of pure MoS_2 and MoS_2@TiO_2 remain stable around the start value. The emission current fluctuation of MoS_2@TiO_2 composites was within ± 4%, owning a slight advantage comparing to MoS_2 nanoflowers, which was within ± 6%. The MoS_2 nanoflowers has been proved to be an excellent candidate for field emission application, the successful coupling of TiO_2 nanoparticles can further protect the emitter from ion bombardment in the operation, thus made MoS_2@TiO_2 a stable field emission material with outstanding property.

3.3 Photocatalytic activites

Currently, the synthesis and morphology control of {001}-faceted TiO_2 is considered to be a focus in photocatalytic studies for the fact that (001) plane with a higher surface energy can be more efficient in dissociative adsorption of the reactant molecules than any other facets.[26] However, since the pure TiO_2 can only be active under UV light irradiation, and the rapid recombination of electrons and holes lowers the quantum efficiency, the idea of doping {001}-faceted TiO_2 with transition metal or metal oxide was conducted by a great number of experiments, aiming to achieve visible light driven photocatalyst as well as semiconductor heterojunctions.[5] The TiO_2@MoS_2 composites were herein synthesized based on the above ideas. A satisfactory photocatalytic activity was observed by monitoring the degradation of MB, which had verified our hypothesis in the first place. Fig. 8 (e) gave the general trend of samples' degradation, and the corresponding absorption spectra of each sample has shown in Fig. 8 (a) (b) (c) (d) respectively. Meanwhile, considering the MB also has the possibility to self-degrade by irradiation without catalyst, we also conducted an experiment as benchmark in order to achieve a rigorous assessment, the result indicated that no degradation was observed in the first 100 minutes, therefore we considered this degradation negligible in our experiment. As we can see from the graph, the TiO_2@MoS_2 exhibited the obvious best photocatalytic activity of 90% within 100 min among the other samples. By comparing the intensity of the main absorption peak of MB, the TiO_2@MoS_2 composites not only shows the strongest adsorption in the dark phase, but also the fastest photocatalytic degradation efficiency, which is defined as C/C_0 where C and C_0 are the remain and initial concentration ratio of MB.

The dash line in Fig. 8 (e) represents the MB concentration after adsorption/desorption equilibrium was established. During this light-off, the MB molecules would anchored on the material's surface therefore were involved in no reaction. The TiO_2-based TiO_2@MoS_2 composites show dramatic increase in adsorption ability from pure TiO_2, on the one hand, MoS_2 grown wave-like on the TiO_2 surface, formed 2D nanosheets rather than 3D nanoflowers, providing an excellent anchoring surface for reactant molecules, on the other hand, the MoS_2 nanosheets grown vertically among the TiO_2 nanorods, result in more gaps, and also a larger specific surface area, which is also consistent with our BET data, indicating that the TiO_2@MoS_2 composites have the largest specific surface area. Due to the fact that the MB molecules did not anticipate in any photocatalytic reaction during the light-off, we can conclude that this significant improvement in adsorption is contributed by the increase in surface area only. Moreover, the TiO_2@MoS_2 composites show an enhanced photocatalytic performance at 666 nm in visible region, which can be attributed to the coupling of MoS_2. Beside the main peak, the photocatalytic degradation at 292 nm which is at invisible region, had also been increased. Fig. 8 (d) shows the MoS_2@TiO_2

Dalton Transactions Accepted Manuscript

This journal is © The Royal Society of Chemistry [year]

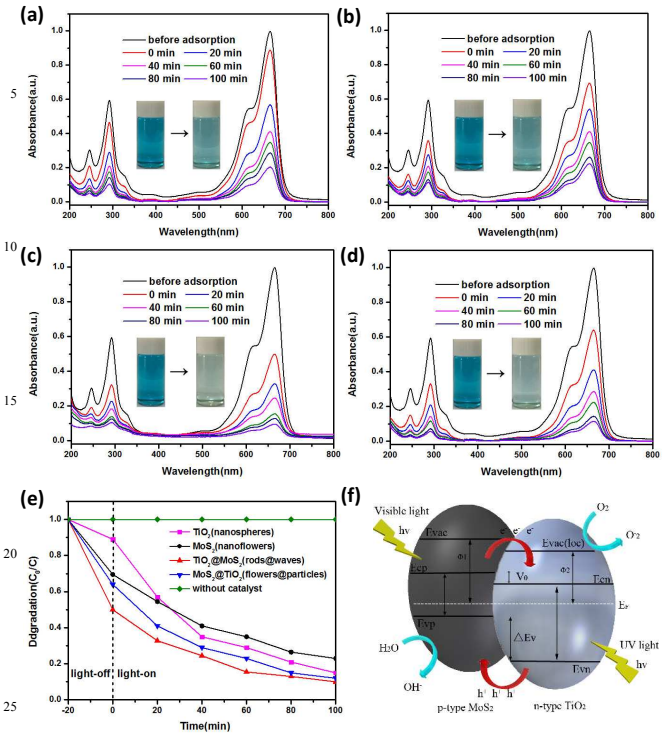

Fig. 8 The absorption spectra and digital decolorization photograph of MB solution at room temperature with the sample of (a) pure TiO2 nanospheres (b) MoS_2 nanoflowers (c) TiO_2@MoS_2 composites (d) MoS_2@TiO_2 composites. (e) The degradation efficiency of four samples within 100 min. (f) the energy band structure of p-n heterojunctions at equilibrium. (EVAC: vacuum level, EF: Fermi level, φ: work function)

also achieved an enhanced photocatalytic properties, but still a lack of adsorption ability and degradation efficiency than TiO_2@MoS_2 composites, which have a better utilization of TiO_2 {001} facets as well as a better contact between two semiconductors.

The enhanced photocatalytic activity of the composites can be explained by the formation of p-n junction, which had been illustrated in Fig. 8 (f). In general, TiO_2 is an n-type wide band gap (3.0 eV) semiconductor with work function of 4.5 eV, while MoS_2 is a p-type narrow band gap (~1.8 eV) semiconductor, with work function of 4.52 eV [30]. The synthesized contact created a heterojunctions structure at the interface between two types semiconductor, the electrons transferred to MoS_2 from TiO_2 until their Fermi levels aligned, also known as the thermal equilibrium state. Because of the carrier concentration gradient, electrons flow from TiO_2 to MoS_2 to form a negative charge, while holes flow from MoS_2 to TiO_2 to form a positive charge, which eventually leads to the equilibrium potential difference (V_0) across the transition region. Based on this contact potential, electron generated at p-type MoS_2 move to the conduction band of n-type TiO_2, and holes generated at TiO_2 diffuse to the valence band of p-type MoS_2 in the photocatalytic process. Therefore, the built–in electric field can significantly reduce the electron-hole pairs' recombination. On the other hand, the separation of electrons and holes' generation effectively benefits the decomposition of the organic dye. The photogenerated electrons reacted with the O_2 and H_2O, and the photogenerated holes can be captured by the H_2O at the catalyst surface, produced powerful superoxide radical like O^{2-}, OH^-, the react mechanism is shown below:

$$TiO_2@MoS_2 + hv \rightarrow e^-(TiO_2) + h^+(MoS_2)$$
$$e^- + O_2 \rightarrow O_2^-$$
$$h^+ + OH^- \rightarrow OH^\cdot$$
$$O_2^- + H_2O \rightarrow HO_2^\cdot + OH^-$$
$$HO_2^\cdot + H_2O \rightarrow H_2O_2 + OH^\cdot$$
$$H_2O_2 \rightarrow 2\ OH^\cdot$$
$$O_2^- / OH^\cdot + MB \rightarrow CO_2 + H_2O$$

To conclude, the increase in quantum yield can be explained by two main factors: first, the built–in electric field which is resulted from the heterojunction structure reduced the electron-hole pairs' recombination, the separation of electrons and holes' generation would eventually benefits the redox reaction with dye molecules. Second, the combination of two semiconductors which have narrow and wide band gap respectively, enlarged the spectrum for light utilization, eventually improved the photocatalytic efficiency.

4. Conclusion

In summary, two kinds of MoS_2 titania heterojunctions were successful synthesized. By reducing the dosage of reactants, the morphologies of MoS_2 and TiO_2 were limited at their primary stage then used to construct composites via two different synthesis directions. The photocatalytic activity and field emission performance were both evaluated. The MoS_2@TiO_2 composites were proved to have a better field emission performance on the account of vast distribution of TiO_2 nanoparticles which were served as sharp edges for emitting, while the TiO_2@MoS_2 composites showed a better photocatalytic performance and adsorption ability due to the large percentage of highly reactive (001) plane of TiO_2 nanorods as well as the increased amount of gaps on the surface. The formation of heterojunctions greatly contributes to the decrease of electron-hole pairs' recombination, which would eventually benefit the performance of both field emission and photocatalytic experiment.

Acknowledgements

The authors acknowledge financial support from the NSF of China (Grant Nos. 61274014, 61474043), Innovation Research Project of Shanghai Education Commission (Grant No. 13zz033), and Project of Key Laboratory of Polar Materials and Devices (Grant No. KFKT2014003).

Notes and references

Key Laboratory of Polar Materials and Devices (Ministry of Education of China), Department of Electronic Engineering, East China Normal University, Shanghai, 200241, P. R. China. Fax: +86-21-54345198; Tel: +86-21-54345198; E-mail: yk5188@263.net

1. A. A. Ismail and D. W. Bahnemann, *Journal of Materials Chemistry*, 2011, **21**, 11686.
2. M. Wang, J. Ioccozia, L. Sun, C. Lin and Z. Lin, *Energy & Environmental Science*, 2014, **7**, 2182.

Dalton Transactions Accepted Manuscript

3. S. H. Hwang, C. Kim, H. Song, S. Son and J. Jang, *ACS applied materials & interfaces*, 2012, **4**, 5287-5292.
4. B. Liu, Q. Wang, S. Yu, P. Jing, L. Liu, G. Xu and J. Zhang, *Nanoscale*, 2014.
5. D. Sarkar, C. K. Ghosh, S. Mukherjee and K. K. Chattopadhyay, *ACS applied materials & interfaces*, 2013, **5**, 331-337.
6. D. Sarkar, C. K. Ghosh and K. K. Chattopadhyay, *CrystEngComm*, 2012, **14**, 2683.
7. T. Cao, Y. Li, C. Wang, C. Shao and Y. Liu, *Langmuir : the ACS journal of surfaces and colloids*, 2011, **27**, 2946-2952.
8. X. Cao, G. Tian, Y. Chen, J. Zhou, W. Zhou, C. Tian and H. Fu, *Journal of Materials Chemistry A*, 2014, **2**, 4366.
9. Q. Gu, J. Long, H. Zhuang, C. Zhang, Y. Zhou and X. Wang, *Physical chemistry chemical physics : PCCP*, 2014, **16**, 12521-12534.
10. M. Wang, L. Sun, Z. Lin, J. Cai, K. Xie and C. Lin, *Energy & Environmental Science*, 2013, **6**, 1211.
11. K. Chang, W. Chen, L. Ma, H. Li, H. Li, F. Huang, Z. Xu, Q. Zhang and J.-Y. Lee, *Journal of Materials Chemistry*, 2011, **21**, 6251.
12. S. Ding, D. Zhang, J. S. Chen and X. W. Lou, *Nanoscale*, 2012, **4**, 95-98.
13. T. Stephenson, Z. Li, B. Olsen and D. Mitlin, *Energy & Environmental Science*, 2014, **7**, 209.
14. C. Song, K. Yu, H. Yin, H. Fu, Z. Zhang, N. Zhang and Z. Zhu, *Journal of Materials Chemistry C*, 2014, **2**, 4196.
15. Y. Wang, S. Li, H. Shi and K. Yu, *Nanoscale*, 2012, **4**, 7817-7824.
16. H. Yin, K. Yu, C. Song, R. Huang and Z. Zhu, *ACS applied materials & interfaces*, 2014, **6**, 14851-14860.
17. H. Yin, K. Yu, C. Song, Z. Wang and Z. Zhu, *Nanoscale*, 2014.
18. X. Xu, Z. Fan, S. Ding, D. Yu and Y. Du, *Nanoscale*, 2014, **6**, 5245-5250.
19. Q. Xiang, J. Yu and M. Jaroniec, *Journal of the American Chemical Society*, 2012, **134**, 6575-6578.
20. W. Zhou, Z. Yin, Y. Du, X. Huang, Z. Zeng, Z. Fan, H. Liu, J. Wang and H. Zhang, *Small*, 2013, **9**, 140-147.
21. J. Li, K. Yu, Y. Tan, H. Fu, Q. Zhang, W. Cong, C. Song, H, Yin and Z. Zhu, *Dalton Transactions*, 2014, **43**, 13136.
22. S. Hu, W. Chen, J. Zhou, F. Yin, E. Uchaker, Q. Zhang and G. Cao, *Journal of Materials Chemistry A*, 2014, **2**, 7862.
23. P. Sun, W. Zhang, X. Hu, L. Yuan and Y. Huang, *Journal of Materials Chemistry A*, 2014, **2**, 3498.
24. X. Wang, J. Ding, S. Yao, X. Wu, Q. Feng, Z. Wang and B. Geng, *J. Mater. Chem. A*, 2014, **2**, 15958-15963.
25. J. Zhou, G. Zhao, B. Song and G. Han, *CrystEngComm*, 2011, **13**, 2294.
26. W. J. Ong, L. L. Tan, S. P. Chai, S. T. Yong and A. R. Mohamed, *Nanoscale*, 2014, **6**, 1946-2008.
27. S. Ding, J. S. Chen and X. W. Lou, *Chemistry*, 2011, **17**, 13142-13145.
28. Y. Ho, W. Zheng, Y. Li, J. Liu and J. Qi *J. Phys. Chem. C*, 2008, 112, 17702–17708.
29. J. Yun, Y. Noh, J. Yeo, Y. Go, S. Na, H. Jeong, J. Kim, S. Lee, S. Kim, H. Koo, T. Kimd and D. Kim, *Journal of Materials Chemistry C,* 2013,**24**, 3777-3783.
30. Y. Liu, Y.-X. Yu and W. D. Zhang, *Journal of Physical Chemistry C*, 2013, **117**, 12949-12957.

Dalton Transactions Accepted Manuscript

This journal is © The Royal Society of Chemistry [year]

Graphical Abstract

Two kinds of MoS_2 titania Nanoheterojunctions with different morphologies was synthesized via different approaches. The excellent field emission performance of the MoS_2@TiO_2 heterojunctions has been obtained for the first time while the TiO_2@MoS_2 heterojunctions possess a better photocatalytic properties.

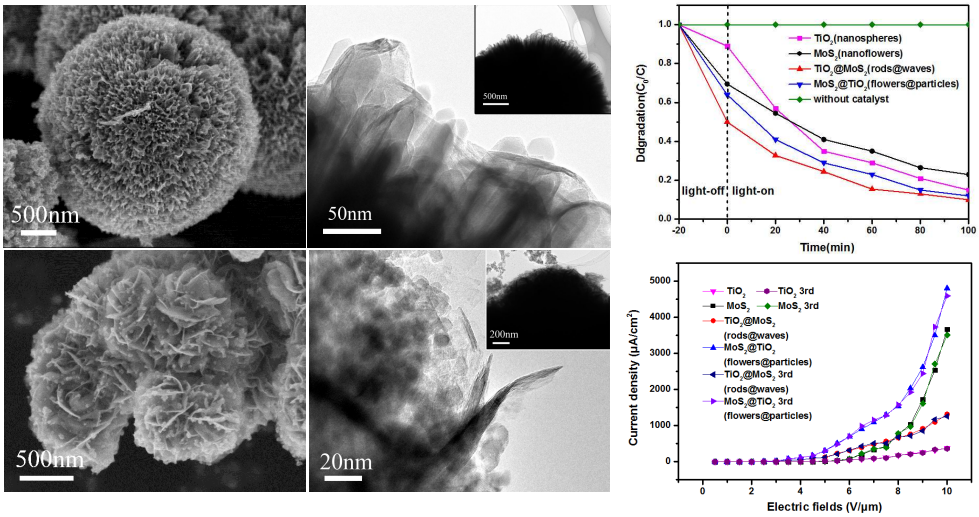

Dalton Transactions Accepted Manuscript